Available online at www.sciencedirect.com
SCIENCE DIRECT
Polymer 46 (2005) 445–453
polymer
www.elsevier.com/locate/polymer

Novel biobased nanocomposites from functionalized vegetable oil and organically-modified layered silicate clay

Hiroaki Miyagawa[a], Manjusri Misra[a], Lawrence T. Drzal[a], Amar K. Mohanty[b,*]

[a]*Department of Chemical Engineering and Materials Science, Composite Materials and Structures Center, Michigan State University, 2100 Engineering Building, East Lansing, MI 48824, USA*
[b]*School of Packaging, Michigan State University, 130 Packaging Building, East Lansing, MI 48824, USA*

Received 28 June 2004; received in revised form 16 November 2004; accepted 17 November 2004

Abstract

The new biobased nanocomposites are processed from anhydride-cured epoxidized linseed oil (ELO)/ or octyl epoxide linseedate (OEL)/diglycidyl ether of bisphenol F (DGEBF) epoxy matrix and organomontmorillonite clay. The selection of anhydride curing agent and biobased epoxy resulted in an excellent combination to provide an epoxy matrix having high elastic modulus, high glass transition temperature, and high heat distortion temperature (HDT), with higher amounts of functionalized vegetable oil (FVO), compared with amine-cured biobased epoxy. The sonication technique was utilized to process the organically-modified clay nanoplatelets in the glassy biobased epoxy network resulting in nanocomposites where the clay nanoplatelets are almost completely exfoliated and homogeneously dispersed in the epoxy network. The processed exfoliated clay nanocomposites showed higher storage modulus compared with the neat epoxy containing the same amount of FVO. Therefore, the lost storage modulus with larger amount of FVO can be regained with exfoliated clay nanoreinforcement.

Keywords: Biobased epoxy; Nanocomposites; Thermo-physical properties

1. Introduction

Research and development of nanocomposites consisting of exfoliated smectite clays in cross-linked polymers have been growing, and the utility of organoclay nanoplatelets in polymers to create nanocomposites having properties greater than the parent constituents has been well reported over the past decade [1]. In these studies, it was found that the nanocomposites have splendid characteristics, e.g. remarkably increased elastic modulus [2–5], creep resistance [6], fracture toughness [7,8], and flammability resistance [9]. Since epoxy resins have a wide range of possible applications in different engineering fields, this paper discusses biobased epoxy/clay nanocomposites, whose glass transition temperature T_g is markedly higher than room temperature (RT). Some present authors have been investigating the mechanical and thermo-physical properties of petroleum-based epoxy/clay nanocomposites prepared by the sonication technique [8,10]. The latter is one of the major techniques to achieve excellent dispersion and exfoliation of clay nanoplatelets in the epoxy matrix. The organoclay is mixed with solvent and either main component of epoxy or hardener. The solvent allows the polymer chain to be absorbed between the clay basal layers and then the solvent is evaporated and removed at high temperature under vacuum. This results in intercalation/exfoliation of clay nanocomposites. It was found that the elastic and storage moduli were increased with exfoliated/intercalated clay nanoplatelets as well as increased glass transition temperature.

Concurrently, the importance of renewable resource-based products for industrial applications becomes extremely clear in recent years with increasing emphasis on the environmental issues, waste disposal, and depleting non-renewable resources. Renewable resource-based polymers can yield a platform to substitute petroleum-based polymers

* Corresponding author. Tel.: +1 517 355 3603; fax: +1 517 353 8999.
E-mail address: mohantya@msu.edu (A.K. Mohanty).

0032-3861/$ - see front matter © 2004 Elsevier Ltd. All rights reserved.
doi:10.1016/j.polymer.2004.11.031

through innovative ideas in designing the new biobased polymers which can compete or even surpass with the existing petroleum-based materials on a cost-performance basis with the added advantage of eco-friendliness. There is a growing urgency to develop and commercialize new biobased products and other innovative technologies that can reduce widespread dependence on fossil fuel and at the same time would enhance national security, the environment, and the economy. Functionalized vegetable oils (FVO), such as epoxidized linseed oil (ELO) and octyl epoxide linseedate (OEL), are now commercially produced by various companies, e.g. Atofina Chemical Company, and these FVO have found applications in coatings and in some cases as plasticizer additives. More value-added applications of such FVO will give much return to agriculture thereby reducing the burden of petroleum-based products. The present authors showed that the blend of petroleum-based epoxy resin and FVO in presence of anhydride curing agent would result in new eco-friendly epoxy materials possibly for highly valuable applications in different engineering fields [11]. It was found that anhydride curing agent was useful to increase the ratio of FVO in the glassy epoxy matrix.

The different properties of the developed biobased epoxy materials can be improved with the addition of nano-reinforcements, such as organoclay nanoplatelets. The incorporation of biobased polymers reinforced by clay nanoplatelets would be one of the best combinations for developing environmentally friendly nanocomposites, if the developed biobased nanocomposites could satisfy the demanding requirements. Therefore, this investigation focuses on glassy epoxy resins having a high glass transition temperature, which is much higher than room temperature. The biobased epoxy nanocomposites containing different FVO were prepared using organo-clay nanoplatelets, and the reinforcing effect of these nanoinclusions on the elastic modulus, and the effect of the organic content of the organo-clay on the glass transition temperature and heat distortion temperature are discussed. The change in the Izod impact strength of the nanocomposites is investigated as well as the failure surface morphology by scanning electron microscopy (SEM).

2. Experimental

2.1. Materials

The main component was the diglycidyl ether of bisphenol F (DGEBF, Epon 862, Resolution Performance Products, Houston TX, epoxide equivalent weight = 172). Two (FVO, ELO Vikoflex® 7190, Atofina Chemicals, Inc., Booming Prairie, MN, epoxide equivalent weight = 176) and OEL (Vikoflex® 9080, Atofina Chemicals, Inc., epoxide equivalent weight = 223) were utilized; 20–100 wt% DGEBF was replaced by the same amount of ELO or OEL in order to obtain novel biobased epoxy matrices. The mixture of DGEBF epoxy and FVO was processed with an anhydride curing agent, methyltetrahydrophthalicanhydride (MTHPA, Aradur™ HY 917, Huntsman Advanced Materials Americas Inc., Brewster NY, equivalent weight = 159) and 1-methylimidazole accelerator, (DY 070, Huntsman Advanced Materials Americas Inc.). The ratio by weight of petroleum-based epoxy resin and FVO to curing agent was adjusted to theoretically achieve stoichiometry. The ratio by weight of mixture of (FVO + DGEBF) and accelerator was fixed as (FVO + DGEBF):DY 070 = 100:1.00.

Organo-montmorillonite clay (Cloisite® 30B, Southern Clay Products, Gonzales TX), a natural montmorillonite modified with methyl, tallow, bis(2-hydrpxyethl) quaternary ammonium (MT2EtOH) ion, was blended in the epoxy using a sonication technique. Nanocomposites were made using clay loading of 5.0 wt%. To fabricate the nanocomposites, the clay nanoplatelets were sonicated by a sonicator (Virsonic 60, The Virtis Company Inc., Gardiner NY) using a sonication probe of 60 watts to agitate the suspension in acetone for 2 h. The sonication procedure was conducted using a mix ratio of 1 kg of clay suspended in 30 l of acetone. The DGEBF and FVO were then added and mixed with a magnetic stirrer for another hour. The acetone was removed by vacuum extraction at approximately 100 °C for 24 h, and then the anhydride curing agent and the accelerator were blended into the solution with a magnetic stirrer. All anhydride-cured biobased epoxy samples were cured at 80 °C for 4 h followed by 160 °C for 2 h.

2.2. Characterizations

2.2.1. Transmission electron microscopy

The exfoliated clay layers in the anhydride-cured epoxy matrix were observed with transmission electron microscopy (TEM). Thin sections of approximately 100 nm thick were obtained at room temperature by ultramicrotomy with a diamond knife having an included angle of 4°. A JEOL 2010 TEM with field emission filament in 200 kV accelerating voltage was used to collect bright field TEM images of the biobased epoxy/clay nanocomposites.

2.2.2. Wide-angle X-ray scattering

Diffraction spectra of wide-angle X-ray scattering (WAXS) were obtained with a Rigaku diffraction system (Cu Kα radiation with $\lambda = 0.15418$ nm) having a monochrometer operating at 45 kV at room temperature. The diffractogram step size was $2\theta = 0.024°$, a count time of 2.88 s and a 2θ range from 1 to 7°.

2.2.3. Dyanamic mechanical analysis

Dynamic mechanical properties including heat distortion temperature (HDT) were collected with a TA Instruments DMA 2980 operating in the three-point bending mode at an

oscillation frequency of 1.0 Hz. DMA specimens were in the form of rectangular bars of nominal size 2.0 mm × 15 mm × 50 mm. Data were collected from ambient to 170 °C at a scanning rate of 2 °C/min. The glass transition temperature, T_g, was assigned as the temperature where loss factor, tan δ was a maximum. A minimum of three specimens of each composition were tested.

Heat distortion temperature (HDT) was also measured in the three-point bending mode. The deflection of the specimens were measured from ambient to 170 °C at a scanning rate of 2 °C/min under a constant load P. The constant load P was calculated as follows:

$$P = \frac{2\sigma t^2 w}{3l} \quad (1)$$

where σ is stress, which is 455 kN/m^2 as recommended in ASTM D 648 standard, l is the span length between two supports in three point bending apparatus (=50 mm), and t and w are the thickness and width of the specimens, respectively. The HDT was defined as a temperature at which the displacement d of the specimen reached the value calculated as follows:

$$d = \frac{\varepsilon l^2}{6t} \quad (2)$$

where ε is strain of the specimen (=0.195%). A minimum of three specimens of each composition were tested to measure HDT.

2.2.4. Izod impact testing

The Izod impact strength was measured for neat epoxy and clay/epoxy nanocomposites at room temperature. Izod impact specimens with the same dimension as prescribed in ASTM D 256 standard were tested with a 453 g pendulum. The dimension of the notched Izod impact specimens was 63.5 mm (length) × 12.7 mm (width) × 10 mm (thickness), and a notch of 1.5 mm depth and 0.25 mm radius was placed along the thickness direction. All specimens were cast from the silicone molds having the same dimensions. The specimen was held as a vertical cantilever beam and was impacted on the notched face by a single swing of the pendulum. Therefore, the crack propagated from the tip of the notch. A minimum of 5 specimens for each composition were tested.

2.2.5. Scanning electron microscopy

The impact failure surfaces of different biobased epoxy nanocomposites were observed with field emission (FE) SEM. A gold coating, which is few nanometers thick, was made on the impact failure surfaces to be observed. A JEOL 6300 SEM with field emission filament in 10 kV accelerating voltage was used to collect SEM images for all samples.

3. Results and discussion

3.1.1. Morphology of clay nanoplatelets

A sample preparation scheme was used to process the organically-modified clay in the glassy biobased epoxy network resulting in nanocomposites where the clay was

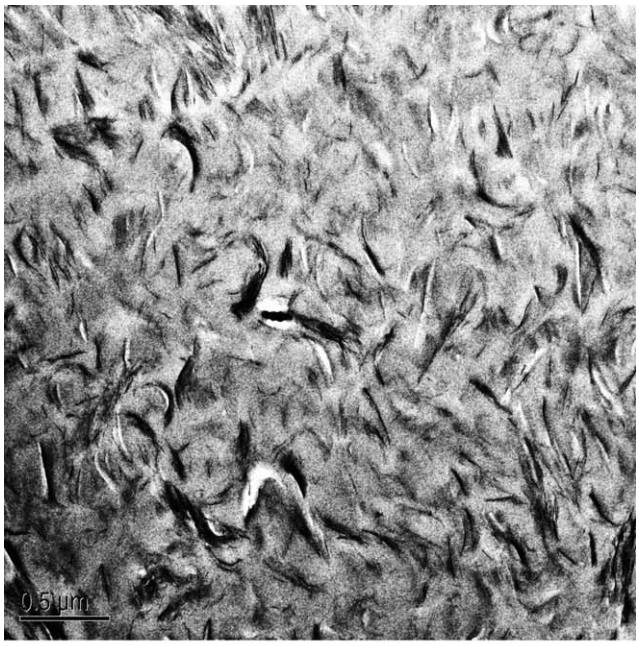

(a)

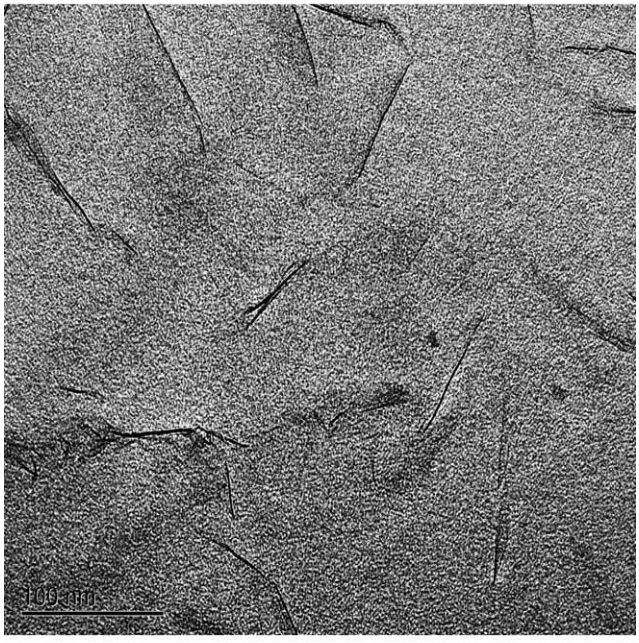

(b)

Fig. 1. Bright-field TEM micrographs revealing homogeneous dispersion and complete exfoliation of 5.0 wt% clay nanoplatelets in biobased epoxy matrix with 20 wt% OEL. (a) Low magnification (scale bar = 0.5 μm); (b) high magnification (scale bar = 100 nm).

almost completely exfoliated by the epoxy network. Fig. 1 shows both low and high magnification TEM micrographs of biobased epoxy/5.0 wt% clay nanocomposites containing 20 wt% OEL. A low magnification TEM micrograph (Fig. 1(a)) shows a general view of the dispersed clay nanoplatelets in the biobased OEL epoxy resin. In Fig. 1(a), the concentration of the clay nanoplatelets seemed to be low and the excellent homogeneous dispersion of clay nanoplatelets was achieved due to the clay modification with MT2EtOH and the sonication process in acetone. Fig. 1(b) presents a close-up view of the completely exfoliated clay nanoplatelets in the biobased OEL epoxy resin. In Fig. 1(b), the d-spacing of clay nanoplatelets could not be identified because of the complete exfoliation. The perpendicular view to the *c*-axis (i.e. along a–b plane) showed typical elongated fiber-like feature. The size of the clay nanoplatelets after the exfoliation was in the range between 50 and 200 nm on the a–b plane, which is markedly smaller than the intercalated clay nanoplatelets [12]. Individual clay nanoplatelets are brittle materials. Therefore, it is easier to break these individual exfoliated clay nanoplatelets, having the thickness of only 1 nm, rather than intercalated clay sticking with a significant number of clay layers. No difference of the clay morphology was observed regardless of different amount of FVO, since all nanocomposites were processed by the sonication technique.

Fig. 2 shows the WAXS patterns at low diffraction angles for organo-montmorillonite clay nanoplatelets and ELO and OEL epoxy/clay nanocomposites prepared with the sonication technique. The [001] diffraction of organo-clay layers before the nanocomposite process appeared at $2\theta = 5.01°$. Therefore, the basal spacing of clay was determined to be 1.76 nm. On the other hand, no clear XRD peak for both bio-based epoxy/clay nanocomposites was observed. Therefore, it could be concluded from both the TEM micrographs and WAXS data that clay nanoplatelets were completely exfoliated. These homogeneous dispersion and complete exfoliation result in the excellent improvement for elastic modulus of clay nanocomposites in the following section.

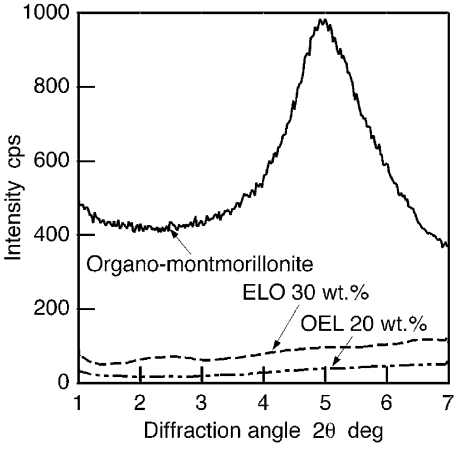

Fig. 2. WAXS patterns of organo-montmorillonite clay and biobased epoxy nanocomposites containing 5.0 wt% clay.

3.2. Density of biobased neat epoxy

Fig. 3 shows the change of the density of the anhydride-cured ELO neat epoxy. The density of the neat biobased ELO epoxy was calculated from the measured weight and size of rectangular bars. The solid circles with standard deviations represent the experimental results and the solid line represents the least squares fit line, respectively. The density of the ELO neat epoxy linearly decreased with increasing the amount of ELO. The result of the least squares fit was used to calculate the theoretical values of the clay volume content of the corresponding nanocomposites having the same amount of ELO. The clay volume content was calculated from the density of the anhydride-cured ELO neat epoxy and density of the clay ($\sim$2.65 g/cm^3). The change of the storage modulus of the biobased epoxy/clay nanocomposites was evaluated by Tandon–Weng equation using the theoretical clay volume content in the following section.

3.3. Thermophysical properties of biobased neat epoxy

The temperature dependency of both the storage modulus and the loss factor of ELO and OEL neat epoxies were measured by DMA. Fig. 4 shows the temperature dependency curve of storage modulus and loss factor of anhydride-cured neat epoxy containing different amount of ELO. In Fig. 4(a), the storage modulus below the glass transition temperature decreased with increasing the amount of ELO. In Fig. 4(b), the peak position of the loss factor curves are approximately 130–140 °C when up to 80 wt% DGEBF was replaced by ELO, although the loss factor peak became broader with the addition of larger amount of ELO. In other words, no clear peak shift was observed in that range of ELO amount. On the other hand, the larger peak shift of the loss factor curve was observed when more than 90 wt% DGEBF was replaced by ELO. These results will be further discussed with the following figures.

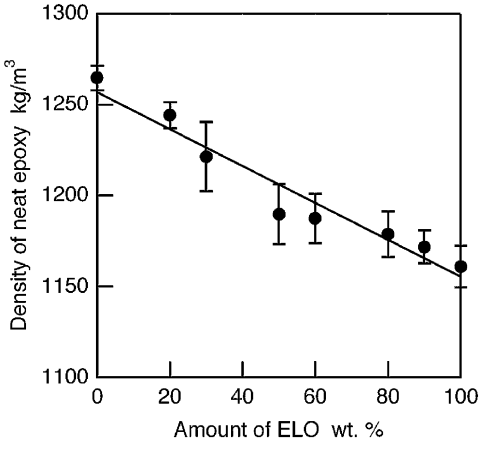

Fig. 3. Change of the density of biobased neat ELO epoxy.

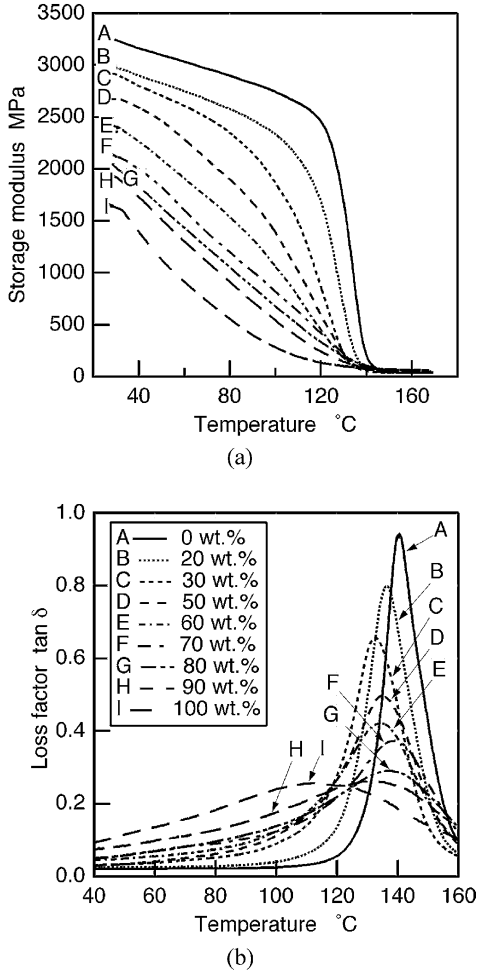

Fig. 4. The effect of ELO concentration for anhydride-cured neat epoxy (captions shared for both Fig. 4(a) and (b)). (a) Storage modulus; (b) loss factor.

Empty symbols in Fig. 5 shows the change in the storage modulus at 30 °C of the anhydride-cured biobased neat epoxies measured by DMA, in respect to regarding the amount of FVO. A dashed line also shows the least squares fit line for neat ELO epoxy. The storage modulus of neat ELO epoxy decreased linearly with increasing the amount of ELO.

Empty symbols in Fig. 6 shows the relation between the glass transition temperature (T_g) determined from the peak position of loss factor curve and the amount of FVO for the anhydride-cured neat epoxies. T_g slightly decreased with increasing the amount of ELO up to 30 wt%, then reached the constant T_g value even if the amount of ELO was increased to up to 80 wt%. It should be noted that the usage of OEL resulted in the lower glass transition temperature, comparing with ELO.

The cross-link density of anhydride-cured biobased neat epoxy was evaluated with DMA data. The cross-link density can be calculated from the following equation:

$$E' = 3\nu_e RT \quad (3)$$

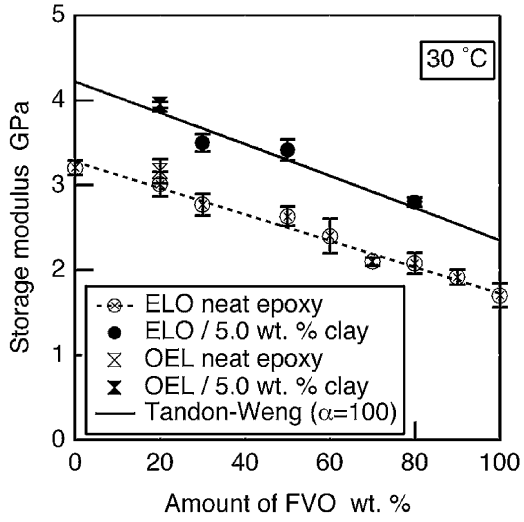

Fig. 5. Change in the storage modulus of anhydride-cured epoxy with FVO and their 5.0 wt% exfoliated clay nanocomposites measured by DMA.

where, E', ν_e, R, and T are storage modulus at (T_g+30) °C, cross-link density, the gas constant (8.314 J/(K mol)), and temperature in K, respectively. Fig. 7 shows the change of cross-link density calculated from the Eq. (3) using the storage modulus at (T_g+30) °C. The cross-link density for anhydride-cured ELO was constant when up to 70 wt% of ELO was added, and consequently, it increased as the storage modulus at (T_g+30) °C increased when more than 70 wt% of ELO was added. It should be noted that the usage of OEL resulted in the lower cross-link density as the glass transition temperature in Fig. 6 decreased more, comparing with ELO.

Fig. 8 shows the relation between peak factor of loss factor curve and the amount of ELO of the anhydride-cured biobased epoxy system. The peak factor is defined as the value of full-width at half maximum (FWHM) divided by

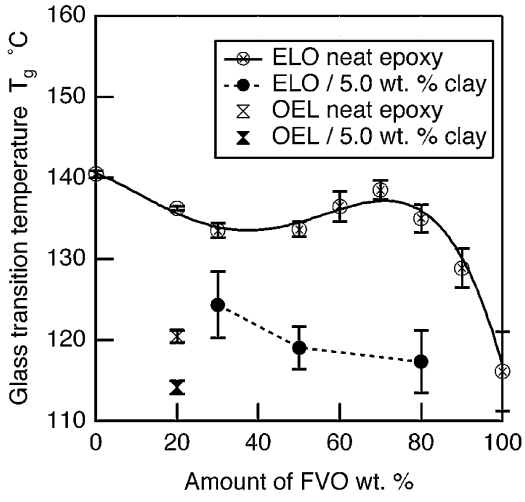

Fig. 6. Change in the glass transition temperature (T_g) of anhydride-cured epoxy with FVO and their 5.0 wt% exfoliated clay nanocomposites measured by DMA.

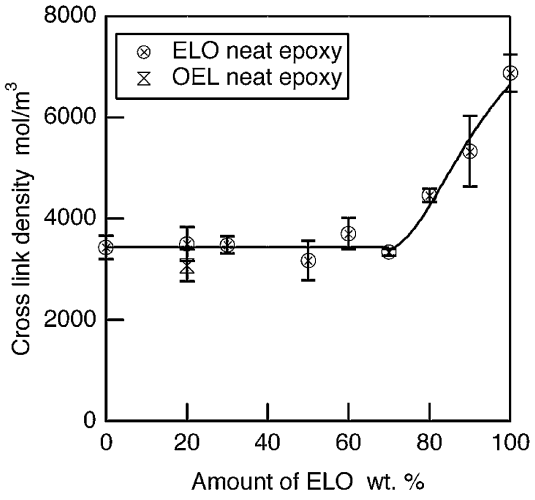

Fig. 7. Change in cross-link density of anhydride-cured neat epoxy with ELO.

the height of the peak. This parameter can give a qualitative assessment of the homogeneity of the epoxy network and the distribution of the molecular weight. Therefore, the broader peak is reflected on the larger value of the peak factor. Empty symbols show the results of the anhydride-cured biobased neat epoxy. A dashed line also shows the least squares line for the anhydride-cured biobased neat epoxy. As can be seen in this figure, the peak factor of the anhydride-cured ELO neat epoxy radically increased with increasing the amount of ELO. Especially in comparing 100% DGEBF and 100% ELO neat epoxy, the difference of the peak factor was almost two orders of magnitude. This suggests that biobased epoxy has broadened glass transition region because of the poor homogeneity of epoxy polymer network. Since vegetable oils have usually a broad molecular weight distribution that generally results in broad peak of loss factor curve, the molecular structure of biobased neat epoxy is more heterogeneous than that of the petroleum-based neat epoxy.

The broad loss factor peak of biobased neat epoxy shown in Fig. 4(b), resulting larger peak factor in Fig. 8, may result in the inaccurate determination of T_g. Therefore, HDT was also measured by DMA to understand the maximum temperature at which the anhydride-cured biobased epoxy materials can be applied as a rigid material. Fig. 9 shows the change of HDT of biobased neat epoxy with respect to the amount of FVO. Differently from T_g, HDT of biobased neat epoxy linearly decreased with increasing the amount of ELO. The HDT of 80 wt% ELO was still higher than 100 °C.

3.4. Thermophysical properties of biobased epoxy/clay nanocomposites

The temperature dependency of both the storage modulus and the loss factor of 5.0 wt% exfoliated clay/biobased epoxy nanocomposites were measured by DMA. Fig. 10 shows the temperature dependency curve of storage modulus and loss factor of anhydride-cured biobased epoxy/clay nanocomposites containing different amount of ELO. In Fig. 10(a), the storage modulus below the glass transition temperature increased with the addition of 5.0 wt% exfoliated clay nanoplatelets for all biobased ELO epoxy. In Fig. 10(b), the symmetric shape of the loss factor curves is indicative to the complete cure of the biobased epoxy matrix. The peak position of the loss factor curves shifted approximately 10 °C lower with the addition of 5.0 wt% exfoliated clay nanoplatelets for all biobased ELO epoxy. These results will be further discussed with the following figures.

Solid symbols in Fig. 5 shows the change in the storage modulus at 30 °C of the anhydride-cured biobased epoxy/5.0 wt% exfoliated clay nanocomposites measured by DMA, in respect to regarding the amount of FVO. The

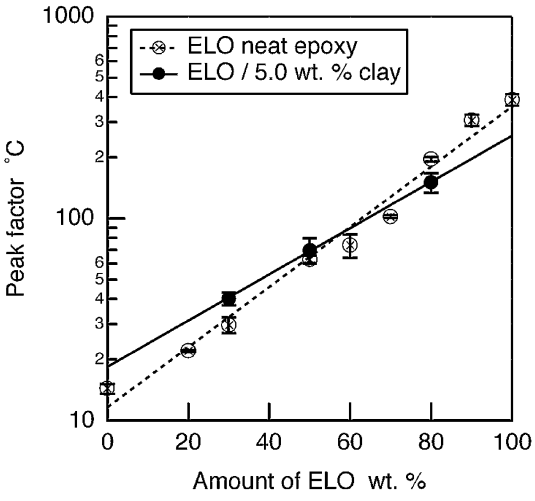

Fig. 8. Peak factor of loss factor curves of anhydride-cured neat epoxy with ELO and their 5.0 wt% exfoliated clay nanocomposites.

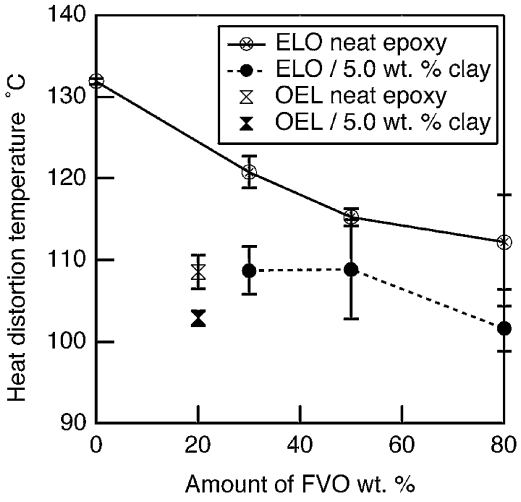

Fig. 9. Change in the heat distortion temperature (HDT) of anhydride-cured epoxy with FVO and their 5.0 wt% exfoliated clay nanocomposites measured by DMA.

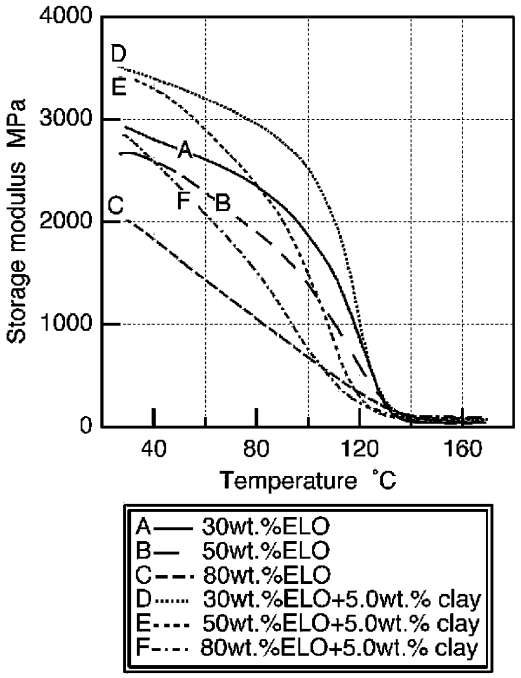

(a)

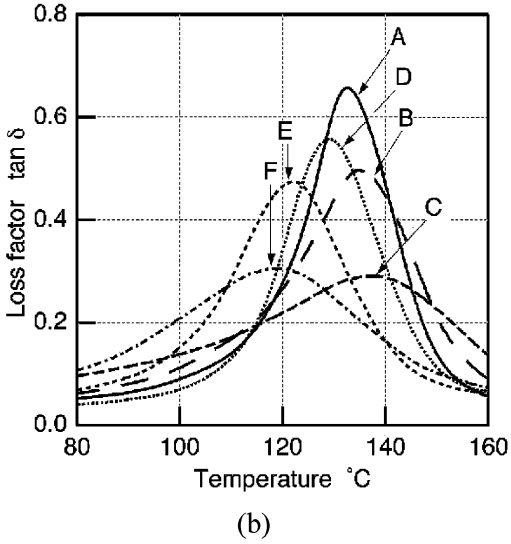

(b)

Fig. 10. The effect of the addition of 5.0 wt% exfoliated clay to anhydride-cured biobased ELO epoxy (captions shared for both Fig. 10(a) and (b)). (a) Storage modulus; (b) loss factor.

biobased epoxy/clay nanocomposites with 5.0 wt% clay exhibited a storage modulus increase at 30 °C of approximately 0.72 GPa relative to the value of the biobased neat epoxy, representing up to 34.7% improvement. This reinforcing effect can be theoretically calculated with Tandon–Weng equation [13] for 3D randomly oriented flake-reinforced composites as a solid line shown in Fig. 5. Some of the authors have already evaluated the storage modulus of intercalated clay nanocomposites using the pseudo-inclusion model [10]. However, as discussed in Figs. 1(b) and 2, the clay nanoplatelets in this study were completely exfoliated in the biobased epoxy matrix. Therefore, the storage modulus of the ELO epoxy/exfoliated clay nanocomposites was evaluated using Tandon–Weng equation for 3D randomly oriented composites without the pseudo-inclusion model. Tandon–Weng equations assume the disc shape for platelets. Organic content in the organo-montmorillonite has been measured as 28.5 wt% by thermogravimetric analysis (TGA). Therefore, when 5.0 wt% organo-clay was added to the biobased epoxy, it was regarded as adding 3.57 wt% neat clay to the biobased epoxy. Consequently, the volume percent of the exfoliated clay nanoplatelets was calculated as approximately 1.6 vol.% using the densities of clay (2.65 g/cm^3) and the experimental value of the density of different ELO neat epoxy shown in Fig. 3. The quantity of a ternary ammonium salt in the organo-clay was extremely small compared with the quantity of the biobased epoxy matrix. Therefore, the change of the density of the biobased epoxy matrix of the exfoliated clay nanocomposites was ignored; the density of the ternary ammonium salt was regarded as the same density of the biobased epoxy matrix. The modulus of clay nanoplatelets was considered as 170 GPa [14]. An average value of the aspect ratio of the exfoliated clay nanoplatelets was estimated with fitting the theoretical line of Tandon–Weng equation to the experimental values. The least square fit line for the storage modulus of the neat ELO was used to evaluate the storage modulus of clay nanocomposites. The theoretical predictions from Tandon–Weng equation shown in Fig. 5 was computed with an aspect ratio (clay length divided by clay thickness) of 100, yielding a extremely close fit to the experimental data acquired by DMA. This theoretically-estimated aspect ratio of clay nanoplatelets was absolutely close to the observed value as discussed in Fig. 1(b).

Solid symbols in Fig. 6 shows the relation between T_g determined from the peak position of loss factor curve and the amount of FVO for the anhydride-cured biobased epoxy/5.0 wt% exfoliated clay nanocomposites. As observed with the anhydride-cured petroleum-based epoxy/clay nanocomposites, which was previously studied by some authors [10], the glass transition temperature of the biobased epoxy/clay nanocomposites decreased because of the quaternary ammonium ion used for clay modification. The clay nanoplatelets used in this study were organically modified, and the organic content, tallow, methyl bis(2-hydroxyethyl) quaternary ammonium ion, was approximately 28.5% by weight. The decrease in T_g is due to the plasticization effect of quaternary ammonium ion in organo-montmorillonite in anhydride-cured epoxy system, which resulted in the lower closs-link density of anhydride-cured epoxy matrix. A long-chain fatty alkyl amine, such as the methyl, hydroxyethyl, tallow-alkyl amine, was released from the organo-clay through simple thermal dissociation during curing. Such a low molecular weight fatty-alkyl amine could readily act as a plasticizer, and hence, lower glass transition temperature was obtained when more organo-clay

was added to the anhydride-cured epoxy system. It was already observed that the nanocomposites with the organo-montmorillonite clay could be cured with only MTHPA without adding any accelerator, and this nanocomposite sample without the accelerator showed even lower glass transition temperature, although the neat anhydride-epoxy mixture did not polymerize without the accelerator.

Solid symbols in Fig. 8 show the relation for the 5.0 wt% exfoliated clay nanocomposites between peak factor of loss factor curve and the amount of ELO. A solid line shows the least squares fit lines to the solid symbols. Interestingly, the peak factor of 80 wt% ELO sample became smaller after adding 5.0 wt% exfoliated clay nanoplatelets. This fact suggests that the excellent dispersion of exfoliated clay nanoplatelets improved homogeneity of biobased polymer network, which can be confirmed by the smaller value of peak factor. For the anhydride-cured ELO epoxy/5.0 wt% exfoliated clay nanocomposites, it can be thought from the cross-section of two least squares lines that this improvement effect due to the exfoliated clay nanoplatelets can occur when more than 60 wt% ELO was added. This improvement may also suggest that the dispersion of exfoliated clay nanoplatelets can avoid phase separation which is observed in epoxy containing different FVO.

Solid symbols in Fig. 9 show the change of HDT with respect to the amount of FVO after adding 5.0 wt% exfoliated organo-montmorillonite clay nanoplatelets. As T_g decreased with increasing clay content as shown in Fig. 6, HDT value also decreased after adding organo-clay nanoplatelets. For the automotive and aeronautical applications, it should be noted that HDT of minimum 100 °C is required. Therefore, it could be thought that the maximum of 50 wt% ELO or 20 wt% OEL might be suitable to process the anhydride-cured biobased epoxy/clay nanocomposites to maintain high HDT value.

3.5. Izod impact strength

Table 1 shows the change of Izod impact strength of the anhydride-cured biobased neat epoxy with different amount of FVO before and after adding 5.0 wt% exfoliated clay nanoplatelets. The standard deviation is shown after ±. The anhydride curing agent processed rigid epoxy samples that have high cross-link density, therefore, the value of Izod impact strength was relatively low. As seen in Table 1, the Izod impact strength of the anhydride-cured ELO and OEL neat epoxy was constant, although the amount of ELO and OEL was changed. This also suggests that the glassy epoxy materials, having high glass transition temperature, were obtained even when the large amount of DGEBF was replaced by ELO or OEL, since rubbery epoxy materials, having low glass transition temperature, show much higher Izod impact strength [15,16]. For the rigid epoxy system, it was reported that it is difficult to maintain the same value of Izod impact strength [8]. Indeed, the Izod impact strength could be maintained after the exfoliated clay nanoplatelets were added to the anhydride-cured FVO epoxy system, as the average value of all sample is indicated in Table 1.

Table 1
Change in Izod impact strength of anhydride-cured neat epoxy with FVO and its 5.0 wt% exfoliated clay nanocomposites

DGEBF (wt%)	FVO (wt%)	Neat epoxy	5.0 wt% Clay nanocomposites
100	0	18.4±3.3	
80	ELO20	16.5±2.5	
70	ELO30	16.4±5.9	16.2±2.0
50	ELO50	16.4±3.5	16.8±3.7
40	ELO60	19.8±3.2	
30	ELO70	12.0±2.9	
20	ELO80	15.2±0.6	18.2±3.9
10	ELO90	12.6±1.9	
80	OEL20	15.9±3.0	15.8±1.1

Fig. 11 shows SEM micrographs of impact failure surfaces of the anhydride-cured biobased neat epoxy containing 50 wt% ELO and its 5.0 wt% exfoliated clay nanocomposites. In Fig. 11(a), the failure surface of the anhydride-cured ELO neat epoxy was extremely flat. This suggests that the behavior of the anhydride-cured ELO neat epoxy was elastic and the crack was propagated in a planer manner under the impact loading, although several small pieces of the epoxy resin were found on the failure surface. The phase separation was not observed, either. Therefore, DGEBF, ELO, and MTHPA were homogeneously mixed and then cured. The similar morphology was observed for anhydride-cured DGEBF and all other biobased epoxy containing different amount of ELO and 20 wt% OEL. The lack of the phase separation resulted in as relatively low Izod impact strength as that of anhydride-cured DGEBF. In Fig. 11(b), the failure surface of biobased epoxy nanocomposites, containing 50 wt% ELO and reinforced by 5.0 wt% exfoliated clay nanoplatelets, showed the rougher surface. Since, phase separation was not observed on the impact failure surface after adding clay nanoplatelets, there was no difference of the Izod impact strength between anhydride-cured ELO and OEL neat epoxy and its 5.0 wt% exfoliated clay nanocomposites.

4. Conclusions

In this paper, the new epoxy based nanocomposite materials were processed with organo-montmorillonite, FVO, and anhydride-curing agent. The selection of anhydride curing agent, ELO, and OEL resulted in an excellent combination to provide biobased epoxy matrices having high elastic modulus, high glass transition temperature, and high HDT with higher amount of FVO in addition to the eco-friendliness due to the utility of the natural resources. The sonication technique was obviously effective to process the organically-modified clay in the glassy ELO and OEL epoxy network resulting in nanocomposites where the clay nanoplatelets were almost completely exfoliated by the epoxy network. The processed exfoliated clay nanocomposites

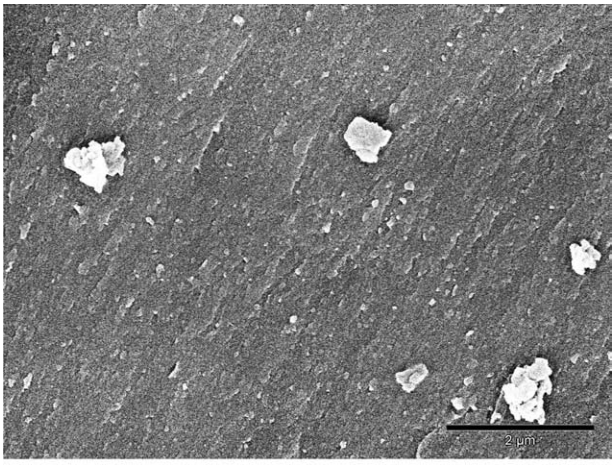

(a)

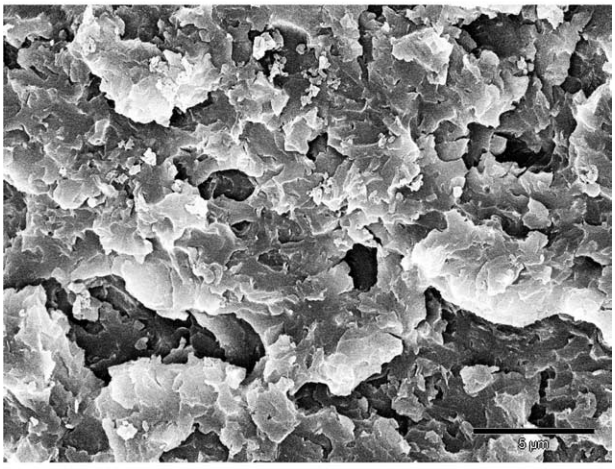

(b)

Fig. 11. SEM micrographs of impact failure surfaces. (a) ELO (50 wt%) neat epoxy (scale bar = 2 μm); (b) ELO (50 wt%)/5.0 wt% exfoliated clay nanocomposites (scale bar = 5 μm).

showed higher storage modulus comparing to the biobased neat epoxy containing the same amount of FVO. Therefore, the lost storage modulus with higher amount of FVO could be regained with exfoliated clay nanoreinforcement. It was possible to achieve 100 °C as HDT. This is a promising fact for possible future industrial applications.

Acknowledgements

The authors are grateful to NSF-PATH (2001 Award No. 0122108) for and Michigan State University's Research Excellence Funds for providing financial support to carry out this investigation. Authors are also thankful to Atofina Chemicals, Inc., Blooming Prairie MN, for the sample supply of the fictionalized vegetable oil samples and Huntsman Advanced Materials Americas Inc., Brewster NY, and Southern Clay Products, Gonzales TX, for the sample supply.

References

[1] LeBaron PC, Wang Z, Pinnavaia TJ. Appl Clay Sci 1999;15: 11–29.
[2] Pinnavaia TJ, Lan T, Wang Z, Shi HZ, Kaviratna PD. In: Chow G-M, Gonsalves KE, editors. Nanotechnology molecularly designed materials, ACS symposium series 622. Washington DC: American Chemical Society; 1996. p. 250–61.
[3] Wang Z, Lan T, Pinnavaia TJ. Chem Mater 1996;8:2200–4.
[4] Lan T, Kaviratna PD, Pinnavaia TJ. Chem Mater 1995;7:2144–50.
[5] Massam J, Pinnavaia TJ. Mater Res Soc Symp Proc 1998;520: 223–32.
[6] Lee A, Lichtenhan JD. J Appl Polym Sci 1999;73:1993–2001.
[7] Zilg C, Muelhaupt R, Finter J. Macromol Chem Phys 1999;200: 661–70.
[8] Miyagawa H, Drzal LT. [in press] J Adhes Sci Technol 2004;(18): 1571–88.
[9] Brown JM, Curliss D, Vaia RA. Chem Mater 2000;12:3376–84.
[10] Miyagawa H, Rich MJ, Drzal LT. J Polym Sci, Part B: Polym Phys 2004;42:4391–400.
[11] Miyagawa H, Mohanty AK, Misra M, Drzal LT. Macromol Mater Eng 2004;289:629–35.
[12] Miyagawa H, Chiou W-A, Daniel IM. Microscopy and microanalysis, vol. 7 (Suppl. 2). Proceedings: microscopy and microanalysis. Long Beach, CA; 2001. pp. 946–947.
[13] Tandon GP, Weng GJ. Compos Sci Technol 1986;27:111–32.
[14] Shia D, Hui CY, Burnside SD, Giannelis EP. Polym Compos 1998;19: 608.
[15] Miyagawa H, Rich MJ, Drzal LT. 31st Annual conference of North American Thermal Analysis Society (NATAS), Albuquerque NM, #109 (CD-ROM); 2003.
[16] Miyagawa H, Mohanty AK, Misra M, Drzal LT. Macromol Mater Eng 2004;289:636–41.